JAAS

PAPER

Cite this: *J. Anal. At. Spectrom.*, 2025, **40**, 1845

Two new barite reference materials for SIMS sulfur isotope analysis: evaluation of the crystallographic orientation effect and homogeneity†

Lan-Lan Tian, [a] Xiao-Lei Wang, *[a] Yue Guan,[a] Wen-Li Xie,[a] Kexin Xu,[a] Feng-Tai Tong,[b] Tao Yang [a] and Yong-Bo Peng[b]

Barite serves as a crucial archive for reconstructing sulfur cycling evolution throughout geologic history. Microscale space variations in sulfur isotope compositions (δ^{34}S) of barite provide valuable insights into the barite precipitation process. While secondary ion mass spectrometry (SIMS) microanalysis has emerged as a powerful tool for such investigations, the availability of high quality reference materials remains a fundamental requirement for accurate measurements. Although several barite reference materials have been developed for SIMS analysis, the potential influence of crystallographic orientation on sulfur isotope measurements has not been systematically evaluated. Moreover, the development of more *in situ* barite reference materials with diverse sulfur isotopic compositions would greatly facilitate cross-laboratory data comparison. In this study, we conducted a comprehensive investigation of the crystallographic orientation effect by combining electron backscatter diffraction (EBSD) and SIMS analyses. Our results demonstrate that crystallographic orientation does not produce significant analytical bias in SIMS barite sulfur isotope measurements at current levels of analytical precision. Furthermore, we present two new well-characterized potential reference materials NJU-Ba-1 and NJU-Ba-2 barite specifically developed for microbeam sulfur isotope analysis. Detailed characterization of texture and major element composition confirms the absence of internal zoning in ground fragments from both barite specimens. These two reference materials establish an extended $\delta^{34}S_{V\text{-}CDT}$ calibration range for microanalytical studies, with certified values of 6.18 ± 0.34‰ (2SD, $N = 17$) and 14.16 ± 0.26‰ (2SD, $N = 9$) for NJU-Ba-1 and NJU-Ba-2 respectively, as determined by gas-source isotope ratio mass spectrometry (GS-IRMS). Extensive SIMS analyses revealed exceptional homogeneity at both inter- and intra-unit scales, with δ^{34}S variations of 0.36‰ (2SD, $N = 328$) for NJU-Ba-1 and 0.45‰ (2SD, $N = 343$) for NJU-Ba-2. These performance characteristics indicate that NJU-Ba-1 and NJU-Ba-2 are promising candidates as reference materials for high-precision microanalytical studies of barite sulfur isotopes.

Received 3rd April 2025
Accepted 17th May 2025

DOI: 10.1039/d5ja00123d

rsc.li/jaas

1 Introduction

Barite ($BaSO_4$) is a chemically stable sulfate mineral characterized by exceptionally low solubility ($K_{sp} \approx 10^{-10}$ at 25 °C), making it a robust geochemical archive across geological timescales.[1,2] As a critical recorder in Earth's sulfur cycle, its sulfur isotopic composition provides unique insights into diverse geological processes.[3–6] Notable applications include: (1) reconstructing the evolution of paleo-oceanic sulfate reservoirs through deep-time records;[3,5–7] (2) preserving anomalous δ^{34}S signatures that serve as biosignatures for early life processes;[8–10] (3) constraining hydrothermal and sedimentary barite ore-forming mechanisms;[11–13] and (4) tracing crust-mantle material recycling in subduction zones through characteristic isotopic fingerprints.[14]

Recent advances in microbeam techniques, including SIMS and LA-ICP-MS (laser ablation multi-collector inductively coupled plasma-mass spectrometry), have significantly improved the spatial resolution of sulfur isotope analysis in barite, allowing for high-resolution reconstructions of dynamic sulfur cycling throughout Earth's history.[15–19] Among these methods, SIMS has become a preferred choice for isotopic microanalysis due to its exceptional spatial resolution. Nevertheless, achieving accurate and precise microanalysis requires high-quality reference materials to correct instrumental mass fractionation (IMF). While two in-house barite reference materials (S0327 and Morvan) have been employed in prior studies,[15,17,20] their homogeneity profiles lacked statistical validation (Table 1). Recent efforts by Li *et al.* (2024) and Lv *et al.*

---

[a] State Key Laboratory of Critical Earth Material Cycling and Mineral Deposits, School of Earth Sciences and Engineering, Nanjing University, Nanjing 210023, China
[b] International Center for Isotope Effects Research, Nanjing University, Nanjing 210023, China. E-mail: wxl@nju.edu.cn

† Electronic supplementary information (ESI) available. See DOI: https://doi.org/10.1039/d5ja00123d

Table 1 Summary of barite sulfur isotope reference materials for microanalysis

		Homogeneity			
Reference materials	δ^{34}SV-CDT (‰, IRMS)	Repeatability (2SD, ‰)	N	Instrument	Reference
S0327	11.0 ± 0.5	Unknown		SIMS	15
Morvan	19.26 ± 0.18	Unknown		SIMS	20
ROM-14898	20.3 ± 0.12	0.30	39	SIMS	21
ROM-48628	21.58 ± 0.33	0.36	48	SIMS	21
ROM-19621	20.13 ± 0.35	0.68	43	SIMS	21
NWU-Brt	14.17 ± 0.42	0.36	50	LA-MC-ICP-MS	22
NJU-Ba-1	6.18 ± 0.34	0.36	328	SIMS	This study
NJU-Ba-2	14.16 ± 0.26	0.45	343	SIMS	This study

(2024) have introduced new reference materials to address this gap (Table 1).[21,22] Despite these advancements, the influence of crystallographic orientation on SIMS barite sulfur isotope analyses remains insufficiently explored. Such orientation effects can introduce significant analytical biases, compromising measurement accuracy and precision.[23–26] For example, in SIMS magnetite oxygen isotope analysis, it has been shown that crystallographic orientation can cause variations up to 2.9‰,[23] a substantial deviation given that routine SIMS oxygen isotope analyses typically achieve precisions better than 0.3‰.[27,28] Therefore, a systematic investigation of crystallographic orientation effects in barite sulfur isotope analysis is critical to obtain reliable and reproducible results. Moreover, developing more *in situ* barite reference standards with a wide range of sulfur isotopic compositions would greatly facilitate cross-laboratory data benchmarking.

In this study, we systematically investigate the influence of crystallographic orientation on sulfur isotope analyses in barite through integrated EBSD and SIMS. First, we employ EBSD to quantitatively characterize the crystallographic orientation distribution of barite fragments. SIMS analyses are subsequently used to precisely evaluate orientation dependent sulfur isotope fractionation effects. Furthermore, we introduce two novel barite reference materials, NJU-Ba-1 and NJU-Ba-2, for sulfur isotope microanalysis. The chemical homogeneity of major elements in these reference materials was verified by electron probe microanalysis (EPMA). Their δ^{34}S values (relative to V-CDT) were precisely determined by GS-IRMS, and repeated SIMS analyses confirm their sulfur isotope homogeneity at the microscale.

2. Sample description

This study investigates two natural barite samples: NJU-Ba-1 and NJU-Ba-2. NJU-Ba-1 was obtained from hydrothermal barite veins during our 2019 fieldwork campaign in the Xiaogang Village of Fengyang County, Anhui Province (32.86°N, 117.53°E) (Fig. 1), with detailed descriptions available in Tian *et al.* (2024).[29] NJU-Ba-2, a pure barite megacryst (Fig. 1), was generously provided by a research collaborator who collected the specimen from a geological survey on the Xiefang Township fluorite deposits of Ruijin County, Jiangxi Province (25.98°N, 116.02°E).

After cleaning, the two natural barite samples were mechanically crushed and sieved through a 75–200 μm mesh, yielding fragments that were subsequently examined using optical microscopy and scanning electron microscopy (SEM). Backscattered electron (BSE) imaging confirmed the exceptional purity of the NJU-Ba-2 fragments, showing no detectable impurities. NJU-Ba-1 fragments show very rare and tiny carbonate inclusions (Fig. 2). The total mass of the handpicked pure barite fragments is approximately 500 g for NJU-Ba-1 and 120 g for NJU-Ba-2.

For microanalytical investigations, we prepared epoxy-mounted sample disks (25.4 mm diameter) containing: approximately 60 NJU-Ba-1 discrete fragments (50–600 μm diameter) distributed across four independent mounts (S061, S068, S089, and S194) and 30 NJU-Ba-2 fragments (50–600 μm diameter) allocated to two distinct mounts (S089 and S194). Fragments were randomly dispersed within a 15 mm central

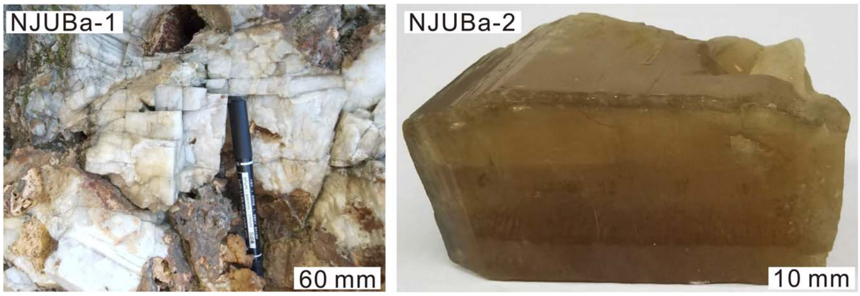

Fig. 1 Photograph of NJU-Ba-1 and NJU-Ba-2 barite.

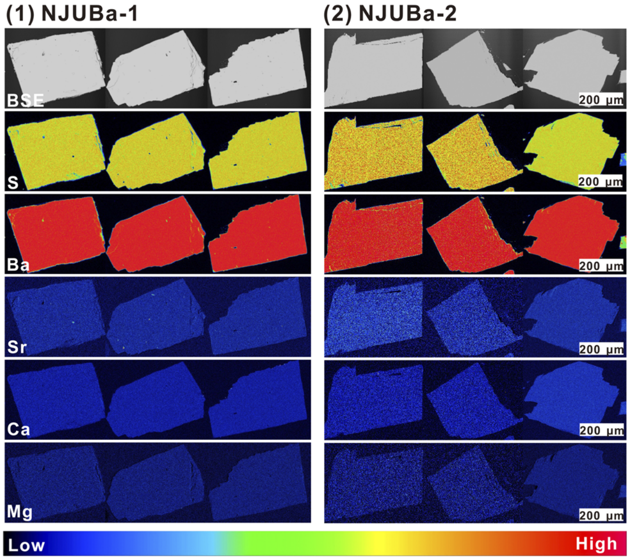

Fig. 2 BSE imaging and major elemental mapping of NJU-Ba-1 and NJU-Ba-2 barite.

analysis zone to minimize edge effects during beam positioning. In addition, some NJU-Ba-1 and NJU-Ba-2 barite fragments were ground to powder (<75 μm) and prepared for bulk analysis.

3 Analytical techniques

3.1. EPMA

Mineralogical analyses were conducted at the State Key Laboratory of Critical Earth Material Cycling and Mineral Deposits, Nanjing University, China. Initial qualitative elemental characterization of NJU-Ba-1 and NJU-Ba-2 was performed using a JEOL JXA-8230 Plus electron probe microanalyzer (EPMA) operating at 15 kV accelerating voltage and 50 nA beam current. Wavelength dispersive spectrometry (WDS) scans were conducted across the 70–230 mm wavelength range, employing a 50 μm step size and 100 ms dwell time per analysis point.

Quantitative major element analysis and elemental mapping were subsequently performed using a JEOL JXA-8530F field-emission EPMA. For quantitative analysis, operating conditions were maintained at 15 kV accelerating voltage, 20 nA beam current, and 5 μm beam diameter, with peak counting times standardized at 10 s for all major elements. Matrix corrections were applied using well-characterized reference materials: barite (BaO and SO_3), amphibole (CaO, MgO, and FeO), crocoite (PbO), chalcopyrite (CuO), and celestite (SrO). Elemental mapping was conducted under optimized conditions of 15 kV accelerating voltage, 50 nA beam current, 0.3 μm step size, and 10 ms dwell time per pixel.

3.2. EBSD

To assess the potential crystallographic orientation effect on SIMS sulfur isotope measurements in barite, we conducted electron backscatter diffraction (EBSD) analysis on an NJU-Ba-1 sample. The EBSD measurements were performed using a Tescan Mira 3 XMU field emission scanning electron microscope equipped with an Oxford Instruments Nordlys EBSD detector at the FiLTER facility, School of Earth Sciences and Engineering, Nanjing University. Analytical conditions were optimized for barite characterization, employing a 70° sample tilt, 20 kV accelerating voltage, and 18–22 mm working distance. Data acquisition utilized a 3.5 μm step size to ensure comprehensive spatial resolution. Diffraction patterns were automatically indexed using Oxford Instruments' Aztec software package. Post-acquisition data processing and visualization were performed using Aztec Crystal software (version 3.1). The analysis generated crystallographic orientation maps and pole figures, which were plotted relative to the major crystallographic axes (100, 010, and 001) within the stereographic triangle. This approach enabled systematic evaluation of lattice preferred orientations (LPO) within the barite fragments.

3.3. GS-IRMS

GS-IRMS analyses were performed at the International Center for Isotope Effects Research, Nanjing University, China. Sample preparation involved encapsulating approximately 0.2 mg of $BaSO_4$ with ~2 mg V_2O_5 in tin capsules. The encapsulated samples were combusted at 1050 °C in a quartz reactor containing an oxygen buffer (Cu + CuO or quartz chips) under a continuous helium flow. The combustion process generated SO_2 along with other gaseous products, which were subsequently separated through a gas chromatography (GC) column before introduction into the mass spectrometer. δ^{34}S measurements were conducted using a Thermo Scientific Delta V Plus mass spectrometer equipped with a continuous flow inlet system. Sulfur isotope measurements were calibrated to Vienna Canyon Diablo Troilite (VCDT, 22.6436) using two in-house barium sulfate standards:[30,31] ICIER-SO-1 (15.05‰) and ICIER-SO-2 (4.05‰). The two in-house standards were calibrated using two international barite standards (NBS127 and IAEA-SO-5 with values of 20.3‰ and 0.49‰, respectively). The standard deviation for both δ^{34}S was better than 0.3‰ based on the performance of the in-house standards.

3.4. SIMS

The SIMS sulfur isotope analysis was conducted using a CAMECA IMS 1300-HR[3] instrument at the State Key Laboratory of Critical Earth Material Cycling and Mineral Deposits, Nanjing University, China. The Cs^+ primary ion beam was operated at 20 keV impact energy in Gaussian mode, delivering a beam current of ~2–3 nA with a resultant spot size of ~20 μm. The 10 μm raster mode was used in the analytical process to reduce the ablation depth, and a normal-incidence electron gun was used for charge compensation. NMR field sensors were applied to stabilize the magnetic field. The magnification of the transfer system was configured as ×75 to increase ion transmission. A 6 × 6 mm width field aperture, *ca.* 122 μm width entrance slit and 50 eV width energy slit were used and the mass resolution constrained by a 500 μm width exit slit on a multi-collector was *ca.* 2400 ($M/\Delta M$, 50% peak width). The ^{32}S and ^{34}S signals were collected simultaneously using two Faraday cups at positions L′2 (10^{10} Ω) and H′2 (10^{11} Ω), respectively. To minimize the effect of FC noise and ensure precise measurements, FC yield and baseline were calibrated weekly throughout the analysis process. The typical count rates were ∼6×10^8 cps for $^{32}S^-$ and ∼2×10^7 cps for $^{34}S^-$, and the internal precision for one spot analysis of the sulfur isotope ($^{32}S/^{34}S$ ratio) was typically ∼0.2‰ (2SE). The total analytical time was approximately 4 min per pit: 80 s of pre-sputtering (to remove the gold coating), ∼60 s of automatic centering of the secondary ions in the field aperture, and a total of 80 s of integration of secondary ions (20 cycles of 4 s integrations).

4 Results and discussion

4.1. Major element compositions of the barite references

The EPMA results and available data suggest that BaO and SO$_3$ dominate the compositions of NJU-Ba-1 and NJU-Ba-2 (Fig. S1 and S2†). While the major element composition of NJU-Ba-1 has been previously reported by Tian *et al.* (2024),[29] our analyses reveal that NJU-Ba-2 has 64.2 ± 0.4 wt% BaO, 35.2 ± 0.3 wt% SO$_3$, 0.48 ± 0.22 wt% SrO, and trace amounts of CaO (0.01 ± 0.01 wt%), FeO (0.01 ± 0.02 wt%), and CuO (0.01 ± 0.02 wt%) (Table 2). Elemental mapping analyses show consistent spatial distribution patterns of major elements across different regions of both barite samples (Fig. 2). Based on the homogeneity of major elements (1SD < 0.4 wt%) and the fact that no compositional zoning is detected at the micrometer scale, it can be concluded that both NJU-Ba-1 and NJU-Ba-2 have excellent chemical homogeneity.

4.2. GS-IRMS $\delta^{34}S$ values of NJU-Ba-1 and NJU-Ba-2

The bulk-rock sulfur isotope compositions of NJU-Ba-1 and NJU-Ba-2 barite powders were determined through repeated analyses, with detailed results presented in Table S1† and Fig. 3.

Table 2 EPMA measurement results for major elements (wt%) in NJU-Ba-2 barite. Data for NJU-Ba-1 barite are reported in Tian *et al.* (2024)[a]

Sample#	SO$_3$	BaO	SrO	CaO	FeO	CuO	MgO	Total
NJU-Ba-1	34.8	64.9	0.04	<LOD	<LOD	0.07	0.014	99.9
NJU-Ba-1	35.0	65.1	0.03	<LOD	<LOD	<LOD	<LOD	100.2
NJU-Ba-1	34.9	64.7	0.08	0.01	0.05	<LOD	0.003	99.7
NJU-Ba-1	34.6	64.7	0.04	0.01	<LOD	<LOD	0.004	99.3
NJU-Ba-1	34.9	64.5	0.03	0.03	0.03	0.01	0.009	99.5
Mean	**34.8**	**64.8**	**0.04**	**0.01**	**0.02**	**0.04**	**0.008**	**99.7**
1SD	**0.2**	**0.2**	**0.02**	**0.01**	**0.02**	**0.04**	**0.005**	**0.3**
NJU-Ba-2	35.6	63.9	0.39	0.00	0.03	<LOD	<LOD	99.9
NJU-Ba-2	35.0	64.3	0.23	0.01	<LOD	<LOD	<LOD	99.5
NJU-Ba-2	34.9	64.3	0.54	<LOD	<LOD	<LOD	<LOD	99.7
NJU-Ba-2	35.1	64.3	0.34	<LOD	<LOD	<LOD	<LOD	99.8
NJU-Ba-2	35.0	64.6	0.40	<LOD	<LOD	0.04	<LOD	100.1
NJU-Ba-2	35.4	63.4	0.91	0.04	<LOD	<LOD	<LOD	99.8
NJU-Ba-2	35.4	64.3	0.52	0.01	0.06	0.02	<LOD	100.4
Mean	**35.2**	**64.2**	**0.48**	**0.01**	**0.01**	**0.01**	**<LOD**	**99.9**
1SD	**0.3**	**0.4**	**0.22**	**0.01**	**0.02**	**0.02**	**<LOD**	**0.3**

[a] <LOD is below the detection limits (CaO < 0.005 wt%; FeO < 0.003 wt%; CuO <0.02 wt%).

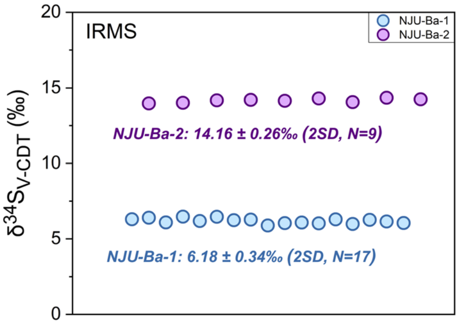

Fig. 3 Isotope ratio mass spectrometry $\delta^{34}S_{V\text{-}CDT}$ results of NJU-Ba-1 and FJ barites. Data are available in Table S1.†

Seventeen replicate measurements of NJU-Ba-1 yielded an average $\delta^{34}S_{V\text{-}CDT}$ value of 6.18 ± 0.34‰ (2SD, $N = 17$), while nine replicate analyses of NJU-Ba-2 produced an average $\delta^{34}S_{V\text{-}CDT}$ value of 14.16 ± 0.26‰ (2SD, $N = 9$). These results demonstrate excellent reproducibility and precision in the sulfur isotope measurements for both reference materials. Compared with previous studies, these two reference materials establish an extended $\delta^{34}S_{V\text{-}CDT}$ calibration range for micro-analysis studies (Table 1).

4.3. SIMS

4.3.1 Accuracy and precision. All SIMS analytical results are comprehensively presented in Tables S2 and S3.† To validate the accuracy of our SIMS sulfur isotope measurements, we conducted comparative analyses using GS-IRMS. During SIMS analysis, NJU-Ba-1 barite served as the primary reference material for instrumental mass fractionation (IMF) correction and long-term stability monitoring, with a determined $\delta^{34}S_{V\text{-}CDT}$ value of 6.18 ± 0.34‰. The IMF-corrected $\delta^{34}S_{V\text{-}CDT}$ value for NJU-Ba-2 barite is 14.23 ± 0.45‰ (2SD, $N = 343$; Table S2,† Fig. 4), demonstrating excellent agreement with GS-IRMS measurements (14.16 ± 0.26‰, 2SD, $N = 9$). Instrumental stability was further confirmed by the minimal $\delta^{34}S$ variation observed in NJU-Ba-1 analyses within each analytical session (≤0.3‰, 2SD; Table S2†). These results collectively demonstrate that our optimized SIMS methodology can produce accurate and precise results of sulfur isotope compositions in barite samples.

4.3.2 Influence of crystallographic orientation on barite $\delta^{34}S$ SIMS measurements. The crystallographic orientation effect on SIMS analyses has been documented across various isotopic systems, including U–Pb geochronology, oxygen isotopes ($\delta^{18}O$), and sulfur isotopes ($\delta^{34}S$), in both oxide and sulfide minerals such as rutile (TiO$_2$),[24] baddeleyite (ZrO$_2$),[25] magnetite (Fe$_3$O$_4$),[23] sphalerite (ZnS),[26] and galena (PbS).[26] Notably, these orientation-dependent biases manifest distinct magnitudes across different mineral systems: magnetite shows $\delta^{18}O$ variations up to 2.9‰ under SIMS analysis,[23] while sphalerite and galena exhibit $\delta^{34}S$ deviations reaching 3.4‰ and 1.7‰, respectively.[26] Such significant analytical biases, comparable to natural isotopic fractionation scales, necessitate

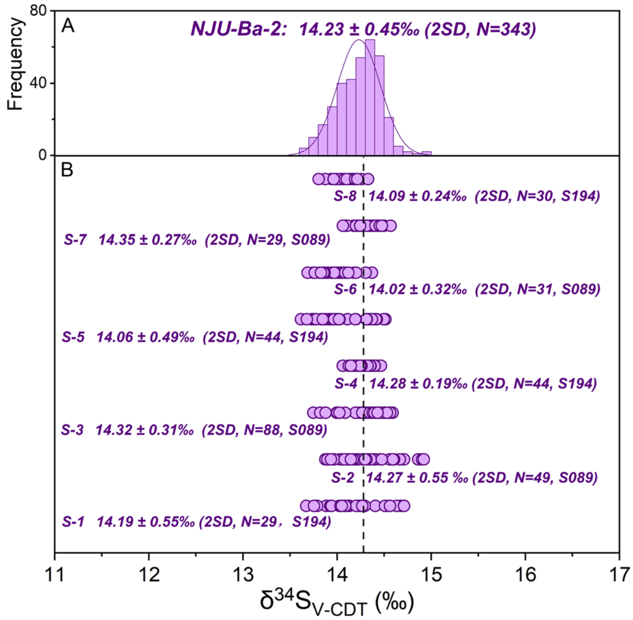

Fig. 4 *In situ* sulfur isotope analysis of NJU-Ba-2 barite: (A) frequency distributions; (B) session resolved $\delta^{34}S_{V\text{-}CDT}$ (‰) calibrated against the NJU-Ba-1 bracketing standard (GS-IRMS: 6.18 ± 0.34‰, 2SD, $N = 17$, Table S1†). ESI in Table S2.†

rigorous investigation of crystallographic orientation effects through standardized protocols involving crystal orientation characterization (*e.g.*, EBSD) and analytical geometry optimization, to ensure metrological reliability in high precision SIMS applications.

Previous studies by Magnall *et al.* (2016) and Li *et al.* (2024) demonstrated consistent sulfur isotope ratios across multiple crystallographic orientations using randomly mounted barite fragments, suggesting minimal orientation effects.[15,21] However, the perfect (001) cleavage plane of barite introduces a potential complication, as fragments naturally tend to align with their cleavage planes parallel to the mount surface during preparation. To rigorously evaluate potential orientation effects in our study, NJU-Ba-1 and NJU-Ba-2 fragments were randomly distributed in epoxy resin mounts. We further conducted EBSD analyses on 45 NJU-Ba-1 barite fragments to quantitatively assess crystallographic orientation distribution.

The resulting crystallographic orientation maps and pole figures revealed a broad, random distribution of crystal orientations (Fig. 5B and C), confirming effective sampling of diverse crystallographic orientations. Supporting SIMS sulfur isotope analyses of 103 spots from these 45 fragments showed minimal variation, with two standard deviations of 0.39‰ ($N = 103$,

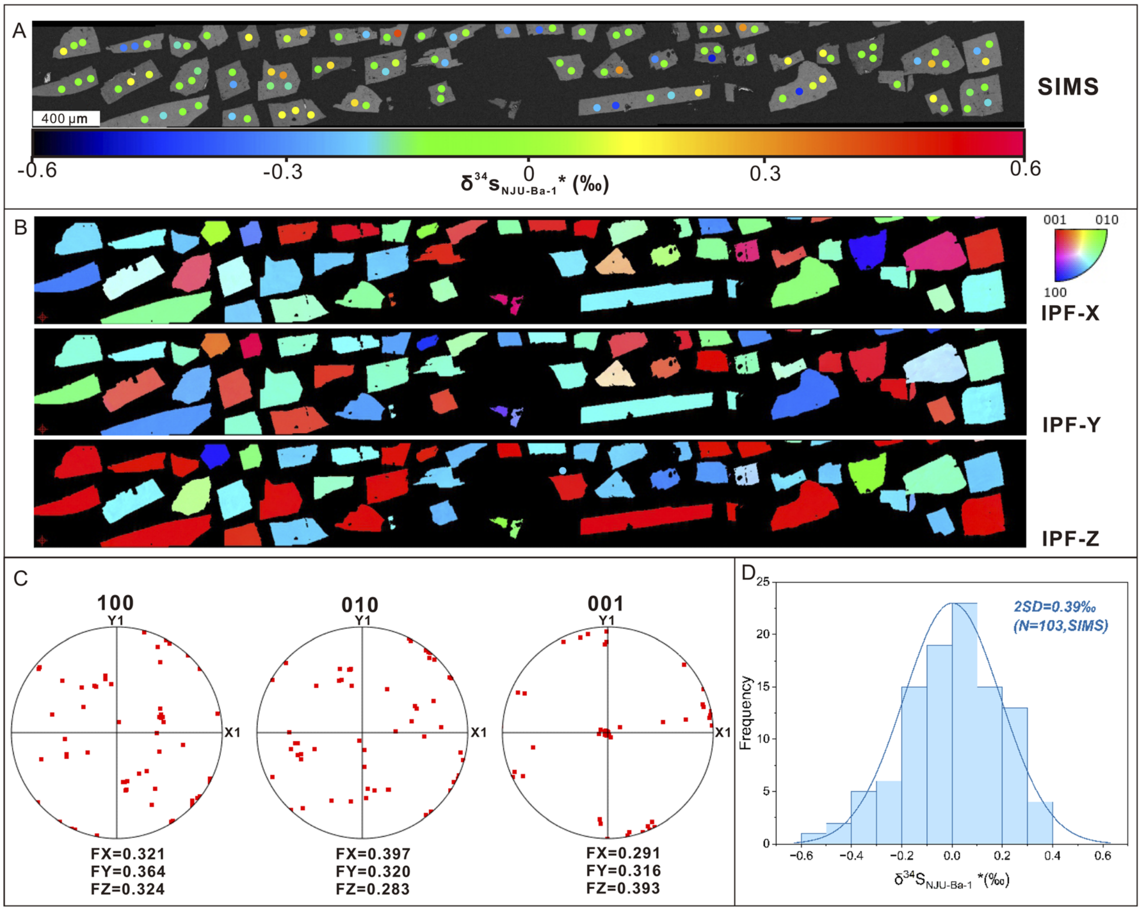

Fig. 5 Evaluating orientation effects of SIMS barite sulfur isotope analysis. (A) SIMS $\delta^{34}S$ values of NJU-Ba-1 barite (Table S3,† Session 1–3); a color scheme is used to correlate $\delta^{34}S$ values to their analytical positions; (B) crystallographic orientation maps for the studied NJU-Ba-1 barite fragments; (C) pole figure maps of NJU-Ba-1 barite fragments; (D) SIMS δ34S values of NJU-Ba-1 barite displayed as a histogram. No correlation between measured $\delta^{34}S$ values and their crystallographic orientations indicates a lack of the orientation effect for SIMS barite sulfur isotope analysis.

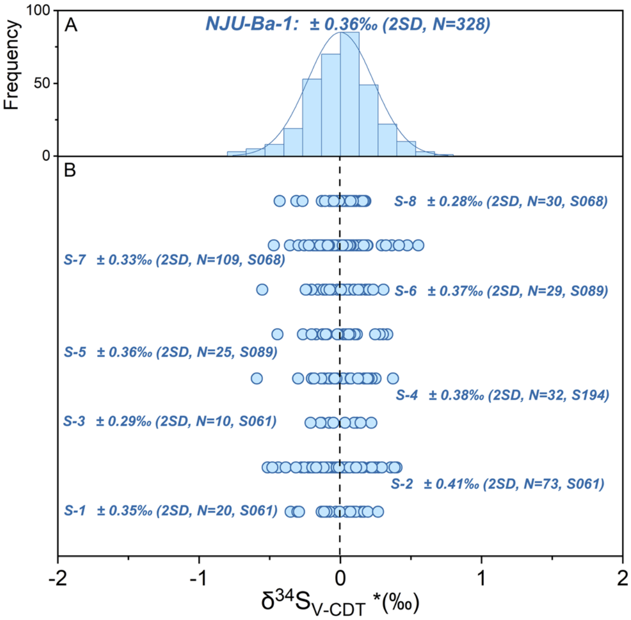

Fig. 6 *In situ* sulfur isotope analysis of NJU-Ba-1 barite: (A) frequency distributions; (B) session resolved analytical precision (2SD) normalized to the mean $^{34}S/^{32}S$ ratio of NJU-Ba-1. ESI in Table S3.†

Table S3,† Sessions 1–3; Fig. 5A and D). The combined EBSD and SIMS data provide robust evidence that crystallographic orientation does not introduce significant analytical bias within the current precision limits (~0.3‰) of our SIMS methodology, validating the reliability of barite sulfur isotope measurements.

4.3.3 Homogeneous sulfur isotope compositions of NJU-Ba-1 and NJU-Ba-2 barite.

Developing homogeneous reference materials is essential for reliable *in situ* microanalysis. This study comprehensively evaluated the sulfur isotope homogeneity of two potential barite reference materials, NJU-Ba-1 and NJU-Ba-2, using SIMS analysis. For NJU-Ba-1, we analyzed 60 fragments across eight analytical sessions, comprising 328 individual measurements (Fig. 6 and Table S3†). The results demonstrate excellent reproducibility (2SD = 0.36‰), with all data points conforming to a Gaussian distribution. In accordance with ISO Guide 35:2017 protocols for homogeneity testing,[32] we conducted a comprehensive evaluation of both inter-unit (between-fragment) and intra-unit (within-fragment) variations through 227 discrete spot analyses performed on 40 randomly selected NJU-Ba-1 fragments (Table S3†). The observed variations were remarkably small, with inter-unit and intra-unit variances of ±0.18‰ and ±0.31‰ (2SD), respectively (Table 3). *F*-Testing confirmed that NJU-Ba-1 barite has exceptional sulfur isotope homogeneity at a confidence level of 95% ($F < F_{\text{critical}}$ for $\alpha = 0.05$, Table 3).[33]

NJU-Ba-2 underwent analogous evaluation, with 343 measurements collected from 30 fragments across eight sessions (Fig. 4 and Table S2†). The material similarly demonstrated robust reproducibility (2SD = 0.45‰) and Gaussian-distributed data. Detailed homogeneity assessment *via* 314 spot analyses on 15 fragments revealed inter-unit and intra-unit variances of ±0.35‰ and ±0.37‰ (2SD), respectively (Table 3).

Table 3 ANOVA statistics for homogeneity testing of sulfur isotope compositions of NJU-Ba-1 and NJU-Ba-2 barite[a]

	NJU-Ba-1	NJU-Ba-2
m	40	15
N	227	314
Q_1	2.59	10.28
Q_2	4.45	8.88
M_{between}	0.07	0.63
M_{within}	0.02	0.03
$2S_{\text{between}}$	0.18	0.35
$2S_{\text{within}}$	0.31	0.37
F	0.58	0.95
F_{critical}	1.46	1.72

[a] m is the number of groups; N is the number of all measurements; Q_1 is the between-group square; Q_2 is the within-group square; M_{between} is the between-group mean square; M_{within} is the within-group mean square; S_{between} is the between-unit standard deviation; S_{within} is the within-unit standard deviation.

F-testing further confirmed no statistically significant heterogeneity in sulfur isotope composition ($F < F_{\text{critical}}$ for $\alpha = 0.05$, Table 3).[33] These comprehensive analyses validate the exceptional sulfur isotope homogeneity of both NJU-Ba-1 and NJU-Ba-2, establishing their suitability as certified reference materials for high-precision *in situ* sulfur isotope microanalysis.

5 Conclusions

This study systematically evaluated the crystallographic orientation effect on barite sulfur isotope analysis through integrated EBSD and SIMS measurements, demonstrating no significant crystallographic orientation related bias within current analytical precision limits. Additionally, we present two well-characterized barite reference materials NJU-Ba-1 and NJU-Ba-2 developed specifically for high precision SIMS sulfur isotope microanalysis. NJU-Ba-1 and NJU-Ba-2 define an expanded $\delta^{34}S_{\text{V-CDT}}$ calibration framework, with GS-IRMS certified values of 6.18 ± 0.34‰ (2SD, $N = 17$) and 14.16 ± 0.26‰ (2SD, $N = 9$), respectively. Both materials exhibit exceptional homogeneity, with long-term reproducibility of 0.36‰ (2SD, $N = 328$) and 0.45‰ (2SD, $N = 343$), respectively. These reference materials are available in substantial quantities for scientific distribution, supporting high-quality microanalytical research.

Data availability

The authors confirm that the data supporting the findings of this study are available within the article and its ESI.†

Author contributions

Lan-Lan Tian: Conceptualization, methodology, investigation, writing – original draft, funding acquisition, and writing – review and editing. Xiao-Lei Wang: Resources, supervision, review and editing. Yue Guan: Investigation. Wen-Li Xie: Investigation. Kexin Xu: Investigation. Feng-Tai Tong:

Investigation. Tao Yang: Resources and supervision. Yong-Bo Peng: Resource, supervision, review and editing.

Conflicts of interest

There are no conflicts of interest to declare.

Acknowledgements

This work was supported by the National Natural Science Foundation of China (42403017) and the State Key Laboratory of Critical Earth Material Cycling and Mineral Deposits, Nanjing University. We appreciate Junyi Pan for providing the NJU-Ba-2 barite, Erkang Qiu and Li Zhang for helping with the EBSD analysis.

References

1 J. S. Hanor, *Rev. Mineral. Geochem.*, 2000, **40**(1), 193–275.
2 G. Y. Wei, H. F. Ling, G. A. Shields, S. V. Hohl, T. Yang, Y. B. Lin and F. Zhang, *Geology*, 2021, **49**(9), 1059–1063.
3 G. Antler, A. V. Turchyn, V. Rennie, B. Herut and O. Sivan, *Geochim. Cosmochim. Acta*, 2017, **203**, 364–380.
4 S. D. Wankel, A. S. Bradley, D. L. Eldridge and D. T. Johnston, *Geochim. Cosmochim. Acta*, 2014, **125**, 694–711.
5 A. Paytan, M. Kastner, D. Campbell and M. H. Thiemens, *Science*, 1998, **282**(5393), 1459–1462.
6 A. Paytan, F. Martinez-Ruiz, M. Eagle, A. Ivy, and S. D. Wankel, 2004. *Sulfur Biogeochemistry - Past and Present*, J. P. Amend, K. J. Edwards and T. W. Lyons.
7 G. Antler, A. V. Turchyn, S. Ono, O. Sivan and T. Bosak, *Geochim. Cosmochim. Acta*, 2017, **203**, 364–380.
8 Y. Ueno, S. Ono, D. Rumble and S. Maruyama, *Geochim. Cosmochim. Acta*, 2008, **72**(23), 5675–5691.
9 G. Antler, A. V. Turchyn, B. Herut and O. Sivan, *Geology*, 2015, **43**(7), 619–622.
10 S. Gong, D. Feng, Y. Peng, J. Peckmann, X. Wang, Y. Hu, Q. Liang, J. Feng and D. Chen, *Chem. Geol.*, 2021, **581**, 12039.
11 S. Sharifiyan, M. R. Hosseinzadeh, S. Maghfouri and M. Moayyed, *Ore Geol. Rev.*, 2021, **139**, 104549.
12 H. K. Hormozi, F. Ehya, G. R. Paydar and S. M. Kheymehsari, *Geochemistry*, 2023, **83**(4), 126024.
13 X. Zhou, R. Li, D. Tang, K. J. Huang, K. Liu and Y. Ding, *Sediment. Geol.*, 2022, **439**, 106220.
14 J. C. Alt, C. J. Garrido, W. C. Shanks III, A. Turchyn, J. A. Padrón-Navarta, V. L. Sánchez-Vizcaíno, M. T. Gómez Pugnaire and C. Marchesi, *Earth Planet. Sci. Lett.*, 2012, **327**, 50–60.
15 J. M. Magnall, S. A. Gleeson, R. A. Stern, R. J. Newton, S. W. Poulton and S. Paradis, *Geochim. Cosmochim. Acta*, 2016, **180**, 146–163.
16 R. S. Wood, A. Lepland, R. C. Ogliore, J. Houghton and D. A. Fike, *Earth Planet. Sci. Lett.*, 2021, **57**, 117164.
17 H. M. Grema, J. M. Magnall, M. J. Whitehouse, S. A. Gleeson and H. M. Schulz, *Front. Earth Sci.*, 2022, **9**, 784824.
18 R. Weibel, H. Vosgerau, M. Larsen, P. Guarnieri, T. F. Kokfelt, K. Dideriksen, T. Balić-Žunić and B. Bell, *J. Sediment. Res.*, 2023, **93**(12), 895–931.
19 J. M. Magnall, S. A. Gleeson and S. Paradis, *Econ. Geol.*, 2020, **115**(5), 953–959.
20 É. Muller, P. Philippot, C. Rollion-Bard and P. Cartigny, *Proc. Natl. Acad. Sci. U. S. A.*, 2016, **113**(27), 7432–7437.
21 B. Li, M. Wiedenbeck, F. Couffignal, A. M. Álvarez-Valero, H. M. Bao, C. F. Fan, J. Han, G. S. Jin, Y. B. Peng, M. D. Syczewski, K. M. Tait, F. F. H. Wilke and U. G. Wortmann, *Geostand. Geoanal. Res.*, 2024, **48**(1), 179–205.
22 N. Lv, Z. Bao, X. Nie, K. Chen, Y. Zhang and H. Yuan, *Geostand. Geoanal. Res.*, 2024, **48**(2), 411–421.
23 J. M. Huberty, N. T. Kita, R. Kozdon, P. R. Heck, J. H. Fournelle, M. J. Spicuzza, H. Xu and J. W. Valley, *Chem. Geol.*, 2010, **276**(3–4), 269–283.
24 R. Taylor, C. Clark and S. M. Reddy, *Chem. Geol.*, 2012, **300–301**(0), 81–87.
25 M. T. D. Wingate and W. Cndmpston, *Chem. Geol.*, 2000, **168**(1–2), 75–97.
26 R. Kozdon, N. T. Kita, J. M. Huberty, J. H. Fournelle, C. A. Johnson and J. W. Valley, *Chem. Geol.*, 2010, **275**(3–4), 243–253.
27 R. B. Ickert and R. A. Stern, *Geostand. Geoanal. Res.*, 2013, **37**(4), 429–448.
28 N. T. Kita, J. M. Huberty, R. Kozdon, B. L. Beard and J. W. Valley, *Surf. Interface Anal.*, 2011, **43**(1-2), 427–431.
29 L. L. Tian, Y. Guan, W. L. Xie, K. Xu, F. T. Tong, T. Yang, Y. Peng and X. L. Wang, *J. Anal. At. Spectrom.*, 2024, **39**(4), 1110–1117.
30 T. Ding, R. Bai, Y. Li, D. Wan, X. Zou and Q. Zhang, *Sci. China, Ser. D:Earth Sci.*, 1999, **42**(1), 45–51.
31 T. Ding, S. Valkiers, H. Kipphardt, P. De Bievre, P. D. P. Taylor, R. Gonfiantini and R. Krouse, *Geochim. Cosmochim. Acta*, 2001, **65**(15), 2433–2437.
32 S. L. R. Ellison and A. Botha, *Accredit. Qual. Assur.*, 2018, **3**, 47–51.
33 J. S. Kane, P. J. Potts, M. Wiedenbeck, J. Carignan and S. Wilson, *Geostand. Newsl.*, 2003, **27**(3), 227–244.